HAL
open science

Influence of Platinum Group Metals particles aggregation on a glass melt rheological behavior

Norma-Maria Pereira Machado, Luiz Pereira, Muriel Neyret, Cécile Lemaitre, Philippe Marchal

To cite this version:

Norma-Maria Pereira Machado, Luiz Pereira, Muriel Neyret, Cécile Lemaitre, Philippe Marchal. Influence of Platinum Group Metals particles aggregation on a glass melt rheological behavior. Journal of Nuclear Materials, 2022, 563, pp.153618. 10.1016/j.jnucmat.2022.153618 . cea-03616919v2

HAL Id: cea-03616919

https://cea.hal.science/cea-03616919v2

Submitted on 31 Mar 2022

HAL is a multi-disciplinary open access archive for the deposit and dissemination of scientific research documents, whether they are published or not. The documents may come from teaching and research institutions in France or abroad, or from public or private research centers.

L'archive ouverte pluridisciplinaire **HAL**, est destinée au dépôt et à la diffusion de documents scientifiques de niveau recherche, publiés ou non, émanant des établissements d'enseignement et de recherche français ou étrangers, des laboratoires publics ou privés.

Influence of Platinum Group Metal particle aggregation on the rheological behavior of a glass melt

Norma Maria PEREIRA MACHADO[a, b*]; Luiz PEREIRA[c] ; Muriel NEYRET[a];

Cécile LEMAÎTRE[b]; Philippe MARCHAL[b].

a CEA, DES, ISEC, DE2D, Univ Montpellier, Marcoule, France

b LRGP, UMR 7274, CNRS-Université de Lorraine, Nancy, France

c Department of Earth and Environmental Sciences, Ludwig-Maximilians-Universität München, Munich, Germany

*norma-maria.pereiramachado@cea.fr

Abstract

Borosilicate glasses are generally used as matrices to immobilize nuclear fission products resulting from spent fuel reprocessing. In the high-temperature vitrification process (1200 °C), most elements to be contained react chemically with the vitrification additives to form a homogeneous glass melt. Platinum Group Metal (PGM) particles are not incorporated chemically in the melt and therefore are present as suspended particles a few microns in size. These particles exhibit an intense aggregation tendency and consequently the suspensions may present an anomalously high apparent viscosity. These systems are characterized by shear-thinning and thixotropic behaviors. However, the interplay between the rheological behavior and the aggregation degree is poorly understood. In this work, the aggregation mechanisms of a simulated nuclear glass melt containing 3.0 wt.% (1.02 vol.%) of PGM particles were investigated. The impact of the shear stress and time on the PGM aggregation degree was determined using an imposed-stress rheometer at high temperature followed by an imaging analysis procedure via Scanning Electron Microscopy (SEM). We present three different aggregation scenarios and their impact on suspension rheology. Based on the experimental data acquired, a force balance computation was performed to illustrate these three scenarios.

Keywords: Melt, Suspension, Platinum Group Metals (PGM), Aggregation, Rheology.

1 Introduction

High-level radioactive waste vitrification is the standard immobilization treatment used in France. After the extraction of uranium and plutonium from spent fuel, the remaining waste is conditioned in a glass matrix in a two-step process. First, the nitrate salts of the waste are converted into oxides at high temperature, yielding calcinate, which is then fed into the melter along with glass frit. This leads to the production of a complex amorphous material that contains around 40 different elements. The melter crucible can be heated by conduction (hot crucible), indirect induction (cold crucible), or in a Liquid Fed Ceramic Melter with electrodes. The nuclear glass is then poured into metal containers and stored in shafts while awaiting future storage in a deep geological repository [1], [2].

Elements and their oxides from the Platinum Group Metals (PGM) (*e.g.*: palladium, rhodium and ruthenium) are insoluble in a nuclear glass melt as well as in the final glass [3]. They are found as palladium-tellurium metallic alloys in a spherical shape (diameter = 1 to 5 μm) together with needle-like ruthenium oxide particles (length ~10 μm), as shown in Figure 1. The presence of these suspended particles has an impact on several physical properties of the glass melt such as the suspension viscosity and electrical conductivity [4]–[7]. In addition, even if the PGM particles are in small amounts (*i.e.*: 3 wt.%), their tendency to aggregate and sediment can lead to the formation of high volume fraction layers at the bottom of the crucible. This can interfere in the process [8][9]. It is important to note that authors observed also abnormal behavior linked to particle aggregation in melt systems containing only RuO_2. Thus, one can state that aggregation is not necessarily directly linked to the presence of Pd-Te particles [10], [11].

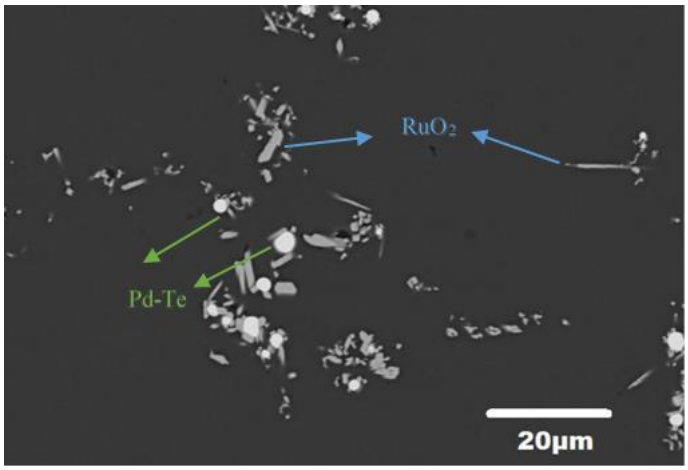

Figure 1 –SEM micrographs taken using back-scattered electrons (BSE) mode under 1000X magnification for the technological nuclear glass containing 3 wt.% PGM particles after vitrification.

It is therefore essential to understand the impact of PGM particles on the physical properties of a nuclear glass melt. In particular, the rheological behavior of a fluid can be strongly influenced by the particle aggregation kinetics as well as the flow, which has an impact on the particles collision and on the dynamics of cluster formation/destruction. Although the PGM particles lead to significant changes in the rheological behavior of their suspensions, the literature on this subject is still limited. Nonetheless, some authors have discovered an increase in the system viscosity in the presence of PGM and a non-Newtonian behavior of the material [4], [8], [12]–[14]. In order to explore the broader shear rate range needed for cold crucible melter development, recent studies have proposed a new phenomenological model for the rheological behavior of these materials [4], [5].

Puig *et al.* (2016) and Hanotin *et al.* (2016) studied the viscosity of simulated nuclear glass melts containing PGM particles as a function of their amounts and temperature [4], [5]. These suspensions presented a shear-thinning behavior and two Newtonian plateaus at low and high shear rates, which were well described by a simplified Cross model:

$$\eta = \eta_\infty + \frac{\eta_0 - \eta_\infty}{1 + (\dot{\gamma}/\dot{\gamma}_c)^m} \quad (1)$$

where η_∞ and η_0 are the viscosity at the high and low shear plateaus respectively, $\dot{\gamma}_c$ is the critical shear rate, at which the shear-thinning transition takes place and m controls the slope of this smooth transition. A previous work have suggested that melts containing PGM particles are well described by m = 1 (simplified Cross model) [15]. At low shear rates and above a certain content of PGM particles, macroscopic aggregates appear. They are made of RuO_2 and Pd-Te chains separated by thin layers of liquid which greatly increase the viscosity of the systems [5]. In this first case, an increase in temperature lowers the viscosity of the melt and improves Brownian diffusion. This in turn favors the particle-particle collision probability leading to an increase of aggregates size and therefore to an overall increase of the suspension viscosity [4]. In contrast at high shear rates, the system behaves as a classical suspension of small clusters and the suspension viscosity is mainly controlled by the liquid phase viscosity that leads to a decrease of the viscosity when the temperature increases.

Particle aggregation can be induced by external and internal factors, but aggregation is an inherent behavior of colloidal systems, even though the extent to which this aggregation prevails may differ widely depending on the particle nature [16]. For molten silicates containing PGM particles, authors [4] have raised a hypothesis that particle aggregation is a result of an interplay of different forces, such as interparticle forces (*e.g.* van der Waals), entropic forces (Brownian motion) and hydrodynamic forces. Several in situ methods are available to study aggregation phenomena by combining rheometry with different characterizations techniques such as ultrasonic velocimetry, X-ray computed tomography, image analysis among others [17]–[19]. Nonetheless, the combination of these techniques is only available at room temperature or below 100 °C, which is much lower than the temperatures of glass melts (900 °C – 1250 °C). In this work, high temperature rheological measurements along with image analyzes was employed to characterize particle aggregation in charged glass melts. The impacts

of time and shear stress on PGM particle aggregation were studied for a simulated nuclear glass melt at 1200 °C. We present here an in-depth analysis of the aggregates and their contribution to the proposed rheological model based on the phenomenology of the system by varying the imposed shear stress and the experiment durations. In this work, we also explore the interplay between the aggregation degree of PGM particles in the melt and the rheological response of suspension.

2 Experimental Method

2.1 Materials

The material used in this study was a simulated nuclear glass containing 3 wt.% of PGM particles. The glass was produced in the full-scale pilot unit installed at CEA Marcoule [20]. The process followed a two-step vitrification protocol at 1200 °C, using the indirect induction technology. The glass was cooled at room temperature and the material studied was extracted from the middle of the canisters. During vitrification, RuO_2 was present in the glass as needle-like of ~10 µm, while Pd-Te alloy appeared as spherical particles with diameters ranging from 1 to 5 µm (Figure 1). The theoretical chemical composition of the nuclear glass is shown in Table 1.

Table 1 – Chemical composition of the nuclear glass samples containing 3 wt.% of PGM particles.

Glass with 3 wt% PGM									
SiO_2 (wt.%)	B_2O_3 (wt.%)	Na_2O (wt.%)	Al_2O_3 (wt.%)	Alkali metal oxides (wt.%)	Alkaline earth metal oxides (wt.%)	Rare earth oxides (wt.%)	RuO_2 (wt.%)	Pd (wt.%)	Others (wt.%)
43.7	13.2	9.2	4.2	3.3	5.0	7.0	1.8	1.2	11.4

2.2 Rheological measurements

Different aggregation degrees were generated by submitting the samples to several shear stresses during different time intervals at 1200 °C, followed by a fast cooling of the sample to "freeze" the particle rearrangements for further image analyses. The high temperature experimental apparatus used for this work is showed in Figure 2 [5]. It consists of a stress-imposed rheometer (Rheometrics Scientific SR5000) above a tubular furnace that could be heated up to 1500 °C. A tool was designed to ensure torque transmission from the rheometer to the crucible without disturbance effects. The characterization cell consisted of an alumina crucible (diameter, height, and wall thickness equal to 27, 40, and 2 mm respectively) previously filled with glass, and centered inside the furnace. The rotor was a multiblade agitator, used in order to maintain a uniform distribution of particles in the glass and avoid settling phenomena [5]. From the top to the bottom of the crucible, the temperature gradient was lower than 2 °C. For these experiments, disposable alumina crucibles were used so that the hardened glass and the crucible could be cut at the end of the experiment in order to analyze the PGM distribution in the glass. The rheological parameters such as shear stress (σ) and shear rate ($\dot{\gamma}$) are linked to measured parameters, namely the torque (C) and the angular velocity (Ω) through geometrical factors K_σ and $K_{\dot{\gamma}}$,

$$\sigma = K_\sigma \, C \qquad \dot{\gamma} = K_{\dot{\gamma}} \, \Omega$$

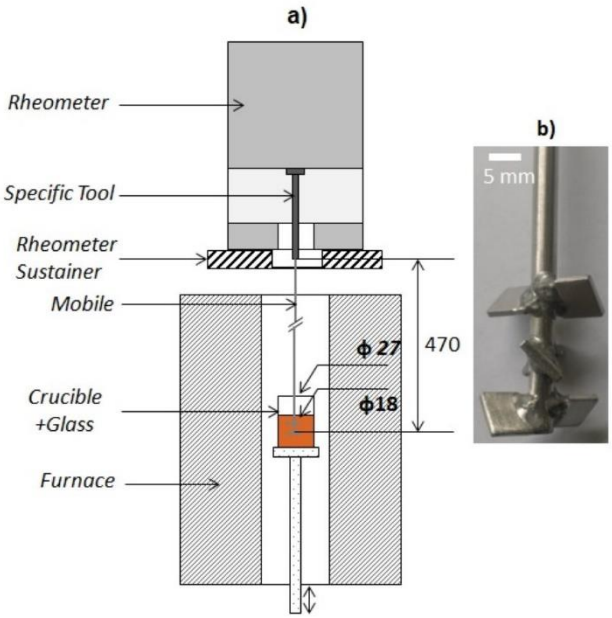

Figure 2- a) High temperature rheological experimental set-up (dimensions in mm), b) Multiblade rotor. [5]

The combination of the crucible and the multiblade geometry formed a virtual Couette cell, therefore factors K_σ and $K_{\dot{\gamma}}$ were determined through a Couette analogy [21] by solving the equation of motion. In the case of Newtonian fluid or a well-characterized power law fluid, the boundary conditions were imposed by the geometrical dimensions of a virtual inner cylinder (the rotor) and the outer cylinder (the crucible) [22]. A complete description of the equipment and calibration procedure was provided in Puig *et al* [5].

In order to establish the overall rheological behavior of the material, a first measurement was made in steady state regime by imposing successive shear stress values, from 0.3 to 300 Pa for 600 s in order to reach equilibrium values. The temporal evolution of the aggregates was then investigated along with the viscosity. In order to create the different aggregation degrees, the measurements were carried out in transient regime by imposing different shear stresses for different times. All samples were first submitted to a pre-shear of 200 Pa for 300 s in order to disperse the PGM particles within the glass melt, which will be referred as the pre-shearing

stage. One crucible that was only submitted to the pre-shear stage was considered as the reference for this study. Then the samples were subjected to a given shear stress, between 0.1 to 200 Pa. The experiment duration for each selected stress was chosen considering the thixotropic behavior of the glass melt. For a given stress level, experiments were performed for 3 to 4 different experimental durations (varying from 300 s to 7200 s). Table 2 shows the shear stresses and time intervals implemented. Each stress/time pair corresponds to a different experiment and to a new crucible, with a total of twenty different experiments.

Table 2 – Operating conditions (shear stress level and duration) for the 20 experiments.

Stress (Pa)	**Duration (s)** (All samples were first pre-sheared at 200Pa for 300s)				
0.1	-	1200	3600	-	7200
2	-	1200	3600	5400	7200
5	300	1200	3600	-	-
10	300	1200	3600	-	-
100	300	1200	3600	-	7200
200	300	1200	3600	-	-

At the end of the rheological tests, the rotor was lifted out of the crucible at a low velocity of 8 mm.min^{-1} to avoid significant changes of particle rearrangement during the withdrawal. The same rotor removal velocity and the same constant speed of crucible cooling were used for all the samples. The crucible was located on an alumina holder that was extracted from the bottom of the furnace. To ensure a compromise between a quick temperature drop and the prevention of thermal shock [23], this descent was conducted at a speed of 2 cm.min^{-1}, equivalent to a cooling rate of 35 °C.min^{-1}. At this rate, no significant changes in the particle rearrangement were expected, due to the rapid increase in the glass viscosity induced by the drop of temperature. In order to observe the impact of withdrawing the rotor on PGM particle distribution, two crucibles were placed in the furnace following the same conditions. The

difference between them was that the first one was placed with no rotor and no agitation and the second one with the rotor but with no applied shear stress.

2.3 Sample preparation

To relieve residual internal stresses introduced in the system during the cooling and to avoid breakage during the sample preparation, the glass underwent annealing at 580 °C for 2 h followed by a slow cooling at 10 °C.h^{-1} until room temperature. To observe the PGM particle distribution in the crucible, it was filled with epoxy resin and cut in half with a circular diamond saw as displayed in Figure 3. One of the halves was cut again horizontally and covered with epoxy resin to fit and to facilitate its support within the SEM measurement cell. The analyzed face was polished and coated with a thin film of carbon for SEM analysis. Each experiment thus produced two samples: the top and the bottom of the crucible (P1 and P2, as shown in Figure 3). The second half of the crucible was kept in case further characterization was needed.

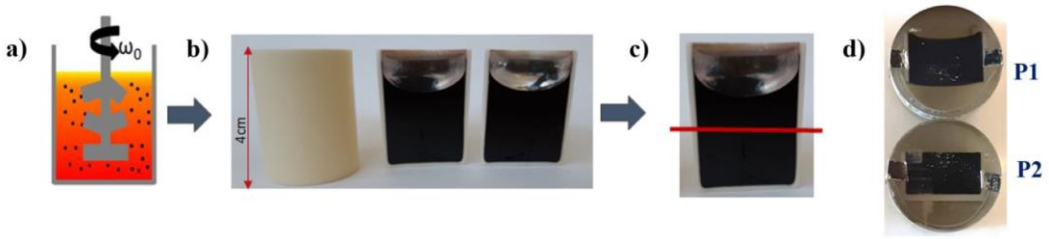

Figure 3 – Samples preparation protocol: the glass melt in the alumina crucible was sheared for a certain time (a). After annealing, the crucible was cut vertically (b), and then cut again horizontally (c), yielding two samples for each crucible (d): top (P1) and bottom (P2).

2.4 Scanning Electron Microscopy imaging

The Scanning Electron Microscopy was performed using a Zeiss Supra 55 FEG. The image of the whole surface was reconstructed from a mosaic of small images automatically acquired using commercial SEM software to describe the PGM particles rearrangement in the most representative area. The most representative zones of P1 and P2 were then selected. To ensure

a standardization of the procedure, the same rectangular region of each crucible was chosen for all experiments. A final area of 1.75 cm² was selected for the bottom and the top samples. The combination of the bottom and top selected surfaces corresponds to the middle of the crucible, *i.e.*, the zone where the rotor was located during the rheological measurement. The analyzed area of the upper sample P1 was located 0.3 cm below the crucible top while the analyzed area of the lower sample P2 was 0.3 cm above the crucible bottom. Each image making up the mosaic was acquired using the back-scattered electron (BSE) mode under a × 100 magnification, a voltage of 15 kV and a 1024 × 768-pixel resolution. Each mosaic contained an average of 320 images, with an acquisition time of ~10 s/image. Due to the size of the sample, a compromise was made between image capture time and resolution. The Fiji software was used for the image processing. The methodology of image acquisition and treatment was derived from crystallization studies involving image analysis found in the literature [24][25]. Subsequently, the information obtained on the PGM particle positions was used as input data to a Python script, developed to quantify the aggregation degree of the samples for different situations under study.

3 Results and Discussion

3.1 Generation of different aggregation degrees

From the first steady state viscosity measurements performed on the glass with 3.0 wt.% of PGM at 1200 °C (Figure 4), six different conditions were selected, expected to produce six different aggregation degrees. The viscosity curve shows three distinct zones displayed in Figure 4: a Newtonian plateau at low shear rates (in blue as M1), a shear-thinning behavior at intermediate shear rates (in green as M2) and a second Newtonian plateau at higher shear rates (in red as M3). Two shear stresses were chosen in each zone, yielding six different

representative stress values, marked with grey stars: 0.1 Pa and 2 Pa in zone M1, 5 Pa and 10 Pa in M2, and 100 Pa, and 200 Pa in M3.

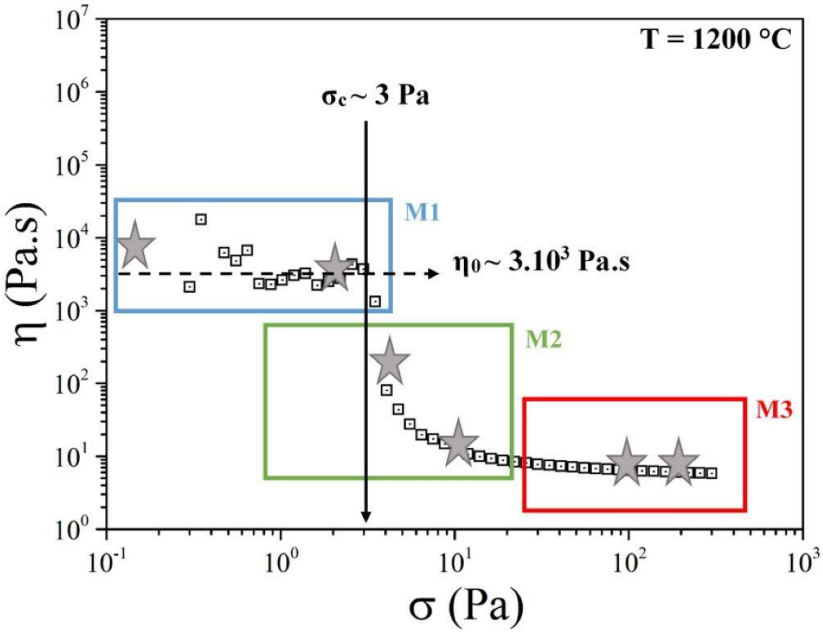

Figure 4 - Evolution of the glass melt viscosity as a function of the shear stress for 3 wt.% of PGM particles at 1200 °C. Stars represent the shear stresses selected for the aggregation analysis.

One of the main limitations of non “in situ” measurements is guaranteeing the reproducibility of the experiment, since for each combination of stress and time, a different sample (in a new crucible) was submitted to the protocol. This is why the tests were repeated at least 3 times, leading to twenty experiments in all. Figure 5 shows the evolution of the suspension viscosity under a shear stress of 5 Pa for three different times: 300, 1200, and 3600 s. These three curves overlap indicating that the three experiments gave the same rheological response so that the methodology reproducibility is guaranteed. It also shows that three main events were captured by the experiments: a sharp increase in viscosity, followed by a more progressive increase and, finally, a stabilization. The thixotropic behavior is more pronounced for the lower stresses, but all the samples studied showed the same reproducibility.

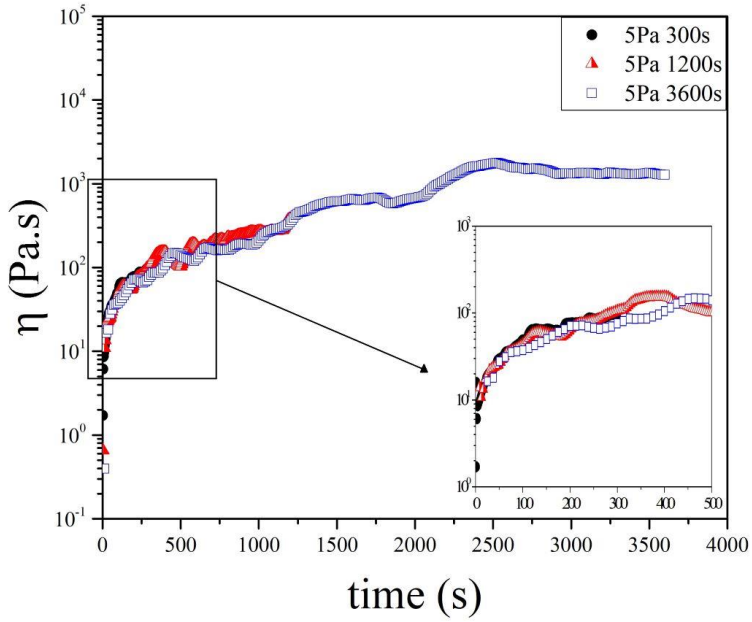

Figure 5 – Evolution of viscosity with time at the imposed stress of 5 Pa for three different samples tested for 300 s, 1200 s and 3600 s. The zoom focuses on the overlap of the three curves, indicating the reproducibility of the experiments.

3.2 Determination of the aggregation degrees

All samples were analyzed using scanning electronic microscopy imaging. For each experiment, images were extracted from the bottom and from the top of the crucible, as mentioned. Although the SEM images give details of the PGM particles in the glass, it is difficult to identify the aggregates only visually. The RuO_2 needles and the Pd-Te spheres were dispersed in the glass matrix normally in groups, as shown in Figure 6a. They are rarely found separately. Therefore, even in the most disaggregated state (after the pre-shearing stage), small clusters composed of RuO_2 needles and Pd-Te spheres remains. It is believed that the pre-shearing scenario (200 Pa, 300s) was not enough to break them all apart. In this current study, these entities are called structural units (SU), and, an aggregate will be a group of SUs close to each other. Thus, if the goal is to observe the aggregation degree of a sample, image processing is necessary to detect the assemblage of these SUs. For this work, the aggregation and dispersion mechanisms will always concern to the union or dispersion of SUs, not the individual RuO_2 and Pd-Te particles. Given that the average diameter size of the SUs measured by SEM

in the glass was ~ 50 µm [14], when the image processing detected larger SUs, it will be considered as a group of SUs, *i.e.* an aggregate.

The image processing consisted in detecting the contours of these SUs so that they could be counted and characterized by the software (Figure 6c). Using the image analyzing, important characteristics of the sample were obtained, such as the total areas and positions of the SUs. Since they did not have a specific shape when grouped, the SUs were analyzed in terms of Féret characteristics (Figure 6d), where their diameters were calculated, as well as the perimeters, mass centers, positions and circularity. These properties obtained by image processing could be used as an approach for defining the aggregation degree of the samples as will be specified later on.

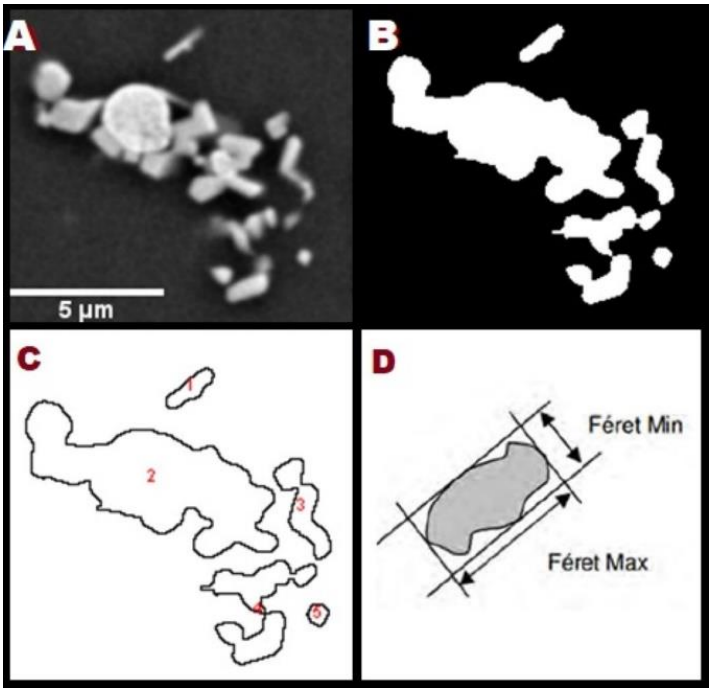

Figure 6 – Example of the image processing applied to the SEM images to identify the structural units of PGM particles: a) Raw image from SEM. b) The same image after processing with the Fiji program. c) Contours of the SUs after processing. d) An example of the Féret form.

Another advantage of the image processing is the contrast created between the particles and the glass matrix by binarizing the mosaic. It produced useful way to visually analyze the

aggregation degree of the samples. Figure 7 shows the mosaics for three samples: i) a sample with no agitation and without rotor (Figure 7a), ii) a sample without agitation and with rotor (Figure 7b), and iii) a sample equivalent to the pre-shear stage (Figure 7c). Based on a visual analysis, a difference in the PGM particle reorganization can be noticed when the rotor was removed from the crucible compared to when there is no rotor (Figure 7a and 7b). The withdraw causes a homogenization of the particles compared to the first scenario. At the same time, the pre-shear lead to a homogeneous dispersion of the SUs in the glass matrix. Although removing the rotor can cause disruption in the PGM reorganization imposed on the sample, it does not produce more aggregation. The only homogenous state that can be considered for all the samples is the pre-shear since it can be imposed on all the crucibles before the measurements.

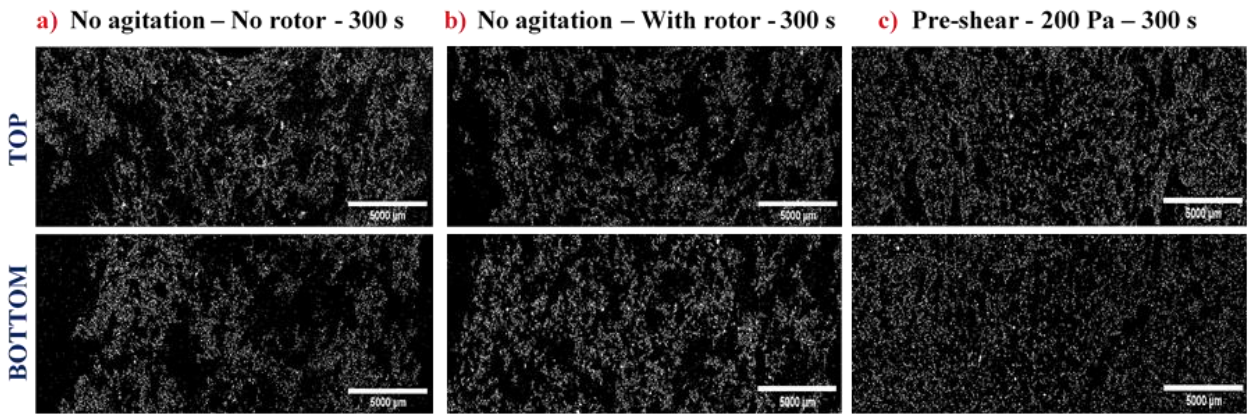

Figure 7 –SEM images of the top and bottom half of the samples, binarized via image processing. a) sample with no rotor and no agitation for 300 s, b) sample with the rotor and no agitation for 300 s, and c) sample submitted to the pre-shear of 200 Pa for 300s. Images b and c were obtained after removing the rotor.

Figure 8 shows an example of the mosaics obtained after image processing for samples subjected to a 5 Pa stress for three different durations (300, 1200, and 3600 s). In the images, the PGM SUs are shown in white (in green on the Cartesian representation) and the glass matrix is black (in white on the Cartesian representation). All samples started from a dispersed state after the pre-shear step (200 Pa for 300 s). As shown in Figure 8a, after 300 s at 5 Pa a slight

rearrangement of the SUs started, but the sample was still homogenous compared to the pre-shear (Figure 7c). The PGM particles regroup more significantly after 1200 s, as shown in Figure 8b, where a large glass matrix area (black) is observed, separating the SUs in large groups. Furthermore, the top and the bottom of the crucible are more heterogeneous than the previous situation. For the last sample (5 Pa stress imposed for 3600 s), the sample is mostly aggregated and the difference between the top and bottom clearly indicates a sedimentation of the particles (Figure 8c). For all the stresses studied, image mosaics were made for each time step (300, 1200 and 3600 s), but the SU evolutions were different. This highlights different mechanisms. The aggregation kinetics were strongly influenced by the imposed stress and the forces acting in the melt. For stresses in a narrow range, these differences may be hard to distinguish using only SEM images. The surface percentage as a function of the SUs diameters was obtained via the image processing for each sample as shown in the fourth column in Figure 8. Although it exemplifies the increase in the SUs diameter over time with a maximum size of 200 µm at 300 s reaching 400 µm at 3600 s, the data is not enough conclusive in how aggregate the sample is. Hence, a numerical tool was necessary to deepen the analysis.

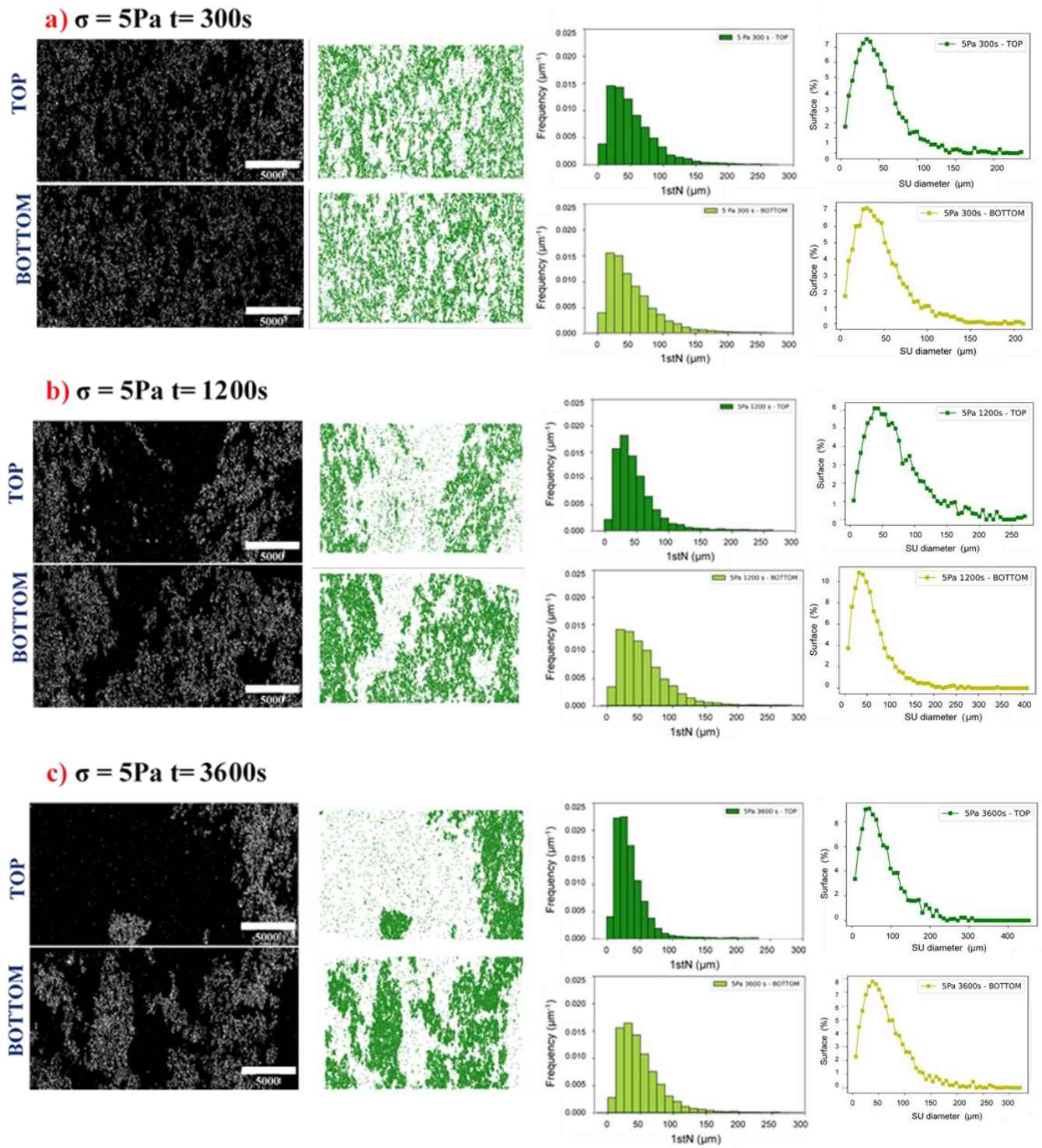

Figure 8 – Top and bottom data of the sample subject to 5 Pa stress for 3 different durations. SEM images (first column) binarized via image processing, along with their corresponding Cartesian representations (second column) of the PGM structural units positioning. Distance of the SUs to their first neighbor (1stN)as a function of their frequency of occurrence (third column) and the surface percentage as a function of the SU diameters (fourth column). Durations of the tests: a) 300 s b) 1200 s, and c) 3600 s.

3.3 Impact of time and shear stress on the aggregation degrees

A Python script was developed to post-process the treated SEM images, in order to quantify the aggregation and the macrostructural characteristics of the suspension. This script uses the Cartesian coordinates of the SUs in the images as input and aggregation parameters are obtained through spatial geometry calculations, in particular the average distance distribution of the SUs to their first neighbor (D1stN). This distance distribution provides an idea of the level of PGM rearrangement and gives information regarding the aggregation degree. In fact, the aggregates are formed by a grouping of SUs that do not necessarily touch one another. The script consists in three steps:

1. Reading the SU positions from the treated SEM image in a Cartesian plane (x,y), and plotting these points as shown in Figure 8 (microstructure in green).

2. Random selection of n SUs belonging to the plotted population of particles.

3. Calculation of the average distance distribution of the SU first neighbors (D1stN) among the chosen n points

The amount of SUs in each image was around 40000 for each of the experiments. In order to limit the computational effort required to evaluate such a large matrix, the calculations were based on n = 8000 random SUs. This value was chosen based on a compromise between the associated error and the required computation time. Since this random number is large enough to represent the whole sample, both aggregated areas and depleted areas in SUs were considered in the computation. The calculation was repeated five times for each image and the standard error associated was calculated. For each stress, two samples were produced from which two D1stN were calculated: one for the top (T) and one for the bottom (B) of the crucible. Figure 9a presents the results for the 5 Pa samples over time. The starting point for all the samples, *i.e.*

t = 0, is the pre-shear. Therefore the D1stN was calculated for the top and the bottom of the crucible submitted to 200 Pa for 300s. As previously mentioned, when analyzing the 5 Pa images a difference was found between the top and the bottom of the crucibles, probably due to sedimentation effects. Nonetheless, the D1stN shows the same evolution in time for both parts of the crucible. If considering the aggregation shown in Figure 8 for the same samples, it is coherent that the distance decreases with time since the SUs are approaching each other. The longer the crucible is submitted to 5 Pa, the more the SUs rearrange to form larger and fewer aggregates.

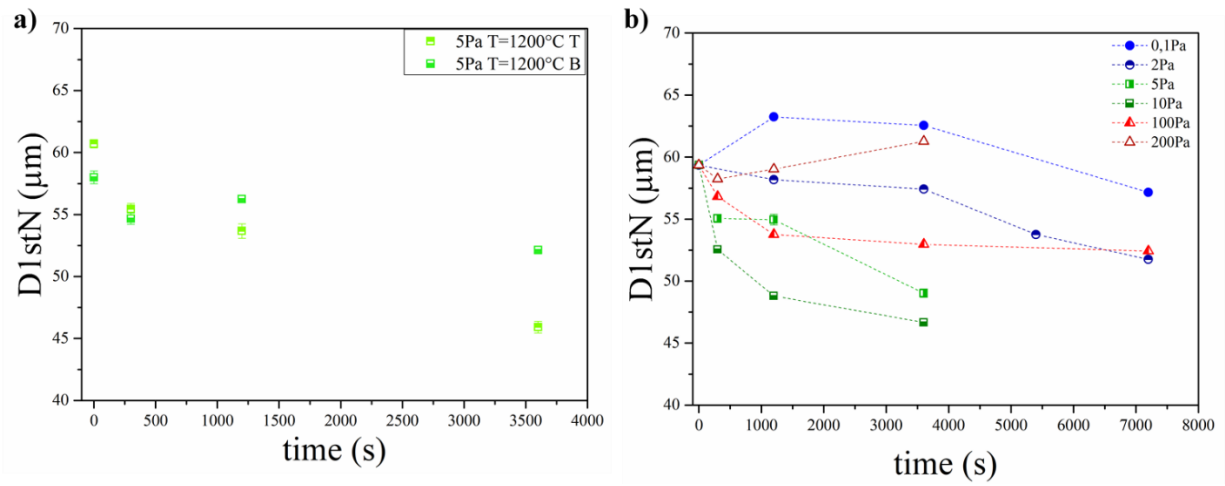

Figure 9- a) Average distance distribution of the SUs first neighbor for the 5 Pa samples as a function of time for the top (T) and the bottom (B) of the crucible. b) Average distance distribution of the SUs first neighbor for all the stresses studied as a function of time.

For all the samples analyzed, both top and bottom of the crucible exhibited the same tendency. The average D1stN was thus calculated for the two crucible parts to indicate the general behavior of the sample. In Figure 9b, the D1stN is shown as a function of the experimental time for all the experiments. All samples start from the pre shear. Firstly, a decreasing of the D1stN with time and with stress can be seen for stresses up to 10 Pa, with the exception of 0.1 Pa which firstly increases and then decreases after two hours under shear. For an imposed stress of 100 Pa, a fast decrease occurred first followed by a stabilization of the D1stN. Lastly, at 200

Pa, the D1stN value increased with time from the beginning of the experiment, and after 3600 s it reached a higher D1stN than the pre shear. By comparing these results with the obtained images, it can be concluded that different aggregation mechanisms govern the PGM particle behavior in the glass melt. The next section will explain these mechanisms in detail.

3.4 Aggregation mechanisms

As shown in Figure 4, the experiments can be separated into three different shear regimes: low shear (M1), medium shear (M2), and high shear (M3). They also represent the different aggregation mechanisms involved in the glass melt. Image analysis alone did not distinguish the aggregation kinetics that the material underwent at each imposed stress. By associating the images with the D1stN, a detailed situation becomes clearer. Figure 10 presents the average distance distribution of the SU first neighbors for all the stresses, in three separate groups. The distance value is normalized by the initial distance (D1stNm) (at time t = 1200 s for 0.1 Pa and 2 Pa, Figure 10a; and t = 300 s for the other stress values, Figure 10b and c) versus the normalized time (t/t_m). t_m is the final experimental time for each situation investigated. The distance points are illustrated by the associated images produced via the Python code as described in section 3.2.

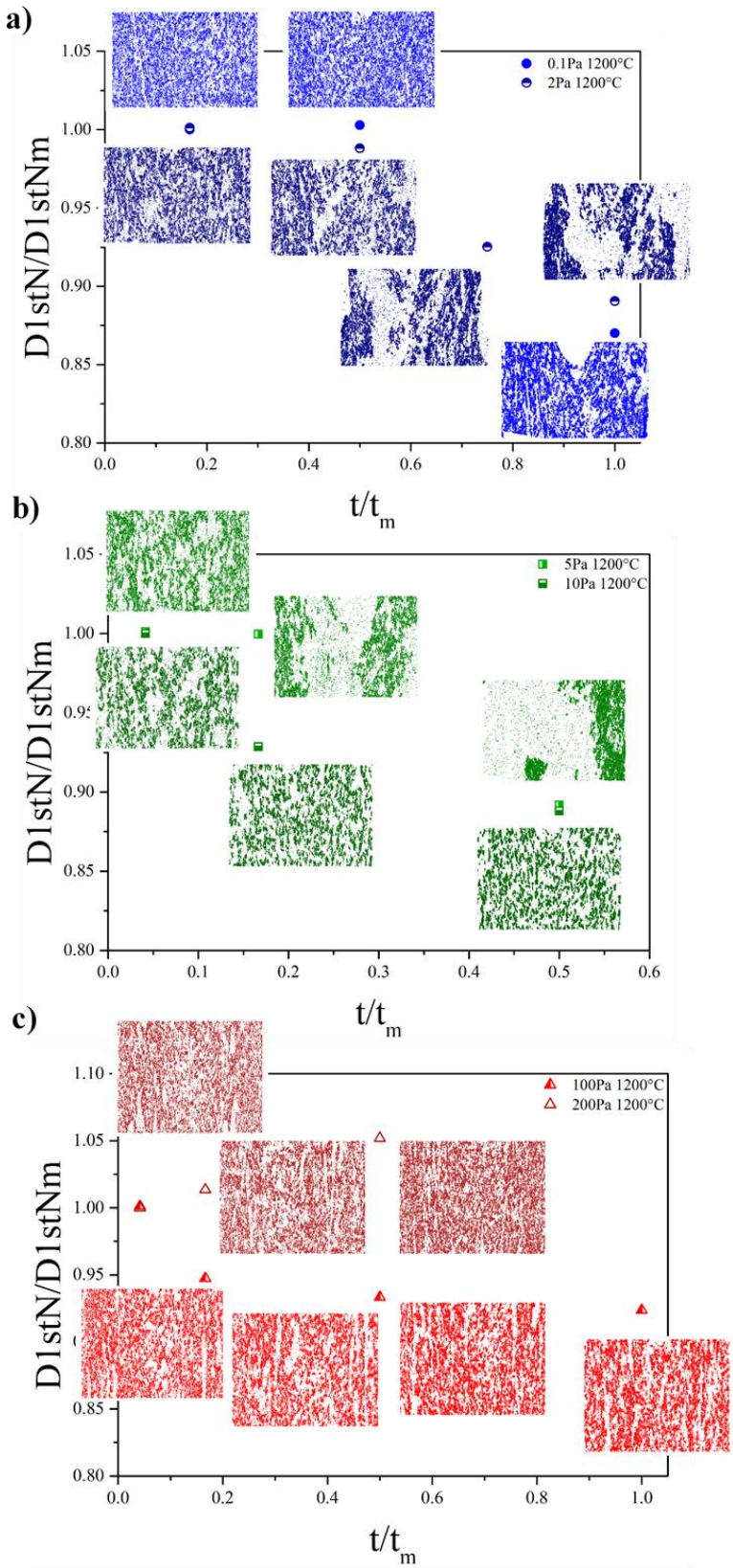

Figure 10 – Normalized D1stN as a function of the normalized time for all stresses studied, separated into three flow regimes, along with the Cartesian representation of the PGM structural unit positioning: a) low shear stress (M1), b) medium shear stress (M2) and c) high shear stress (M3).

To interpret the behavior, this discussion is based on the so-called DLVO (Derjaguin, Landau, Verwey, and Overbeek) theory [26], [27]. This theory was developed to explain the aggregation of aqueous dispersions. In the DLVO theory, aggregation of dispersed particles is explained by the interplay between the attractive van der Waals and the repulsive electrostatic double-layer force. Van der Waals forces between identical particles are always attractive and consequently promote aggregation, while electrostatic double-layer force stabilizes the dispersion, keeping identical particles apart. Their intensities do not depend on the external shear rate imposed by the rheometer. Thus once aggregation is taking place it can be seen that attractive forces predominate over repulsive ones. However, in the case studied here, the shear stress imposed by the rheometer generated hydrodynamic forces that, depending on their intensities, could either favor or prevent the aggregation of PGM particles, as will be shown next.

For the low shear stress regime (M1, Figure 10a), a decrease in the normalized D1stN with time can be noted for both stresses. In this regime, the hydrodynamic forces imposed by the rheometer are weak and not strong enough to push the particles away from each other, so that van der Waals attraction dominates in this situation. Therefore in the M1-scenario, SUs could undergo aggregation and larger SUs were formed. Focusing on the images at $t/t_m = 1$ under low shear stresses, the sample at 2 Pa exhibits an obvious heterogeneity. This indicates that for this shear stress range, the low hydrodynamic forces promote collisions and favor aggregation. In this first regime, the higher the stress, the quicker the aggregation kinetics leading to a smaller distance between the SUs (D1stN). This rearrangement is correlated with the Newtonian plateau at low shear, which was observed in the steady state rheological tests (Figure 4). Particle-particle interactions that lead to aggregation have dramatic effects on viscosity, since the resulting aggregates are larger than individual particles and so immobilize some of the liquid phase, increasing their effective volume fraction. This results in a higher viscosity at low shear

rates that increases with temperature despite the resulting decrease in the matrix viscosity [28][29].

Figure 10b shows the results for the medium shear stress regime (M2). This shear range is characterized by a decrease in viscosity with increasing shear stress when compared to the low shear regime M1. However, the same trend as the one previously described for the M1 regime can be observed: for a given shear stress, D1stN decreases with the run duration. Although the dependence is the same, the difference lies in the kinetics of the phenomenon. When the shear is increased above a critical stress, hydrodynamic forces increase enough to counteract the aggregation phenomena, controlled by Brownian diffusion. The shear stress imposed is not high enough to completely disperse the SUs, but it enhanced the local reorganizations. Unlike the first mechanism, when the stress increased, the aggregate size reached after one hour decreased.

At a given shear stress or shear rate, the steady state is reached when a dynamical equilibrium is established between the breakdown and building of aggregates, leading to a mean equilibrium of the radius. The aggregate will reach its maximum equilibrium size at the maximum imposed stress that it can support without breaking [30]–[32]. This radius will decrease as the shear increases, and consequently the viscosity will also decrease. Even though the aggregates are smaller, the distance between SUs keeps decreasing. This is due to a competition between cohesive forces caused by the fluid and rupture forces caused by the flow [33].

The results concerning the third regime (regime M3) are presented in Figure 10c. This regime is also characterized by a Newtonian plateau at high shear on the steady state rheograms. Contrary to mechanism M1 explained earlier, in which aggregation dominates, at high shear flow scenarios, the hydrodynamics forces are higher than the interparticle forces controlling

then the behavior of the suspension, leading to the rupture of the aggregates [34]. The distance between the SUs stabilizes over time at this range. As shown in Figure 10c, the PGM SUs are completely dispersed in the glass matrix. This dispersion leads to greater first neighbor distances for the SUs compared to the other regimes.

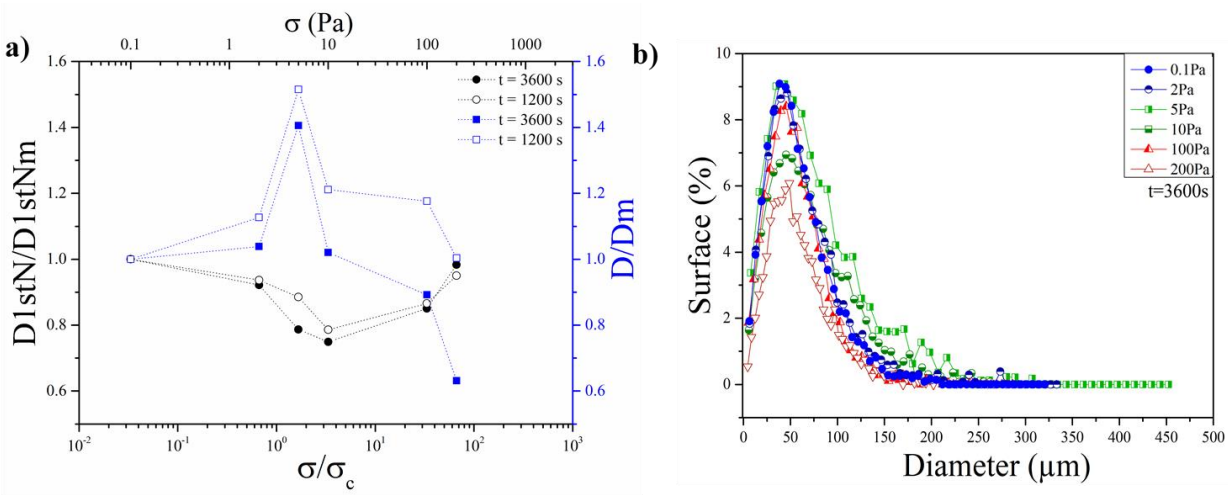

Figure 11 – a) Normalized D1stN and normalized Féret diameter (D) as a function of the normalized shear stress for experimental durations t = 3600 s and t = 1200 s. D1stN/D1stNm and D/Dm are represented by the circles and squares, respectively. b) Surface percentage as a function of the SU diameters for all the 3600s-samples studied.

In order to analyze the overall impact of shear stress in the material aggregation degree, the three regimes were compared at two experimental durations for varying applied shear stress. Figure 11a shows the dependency of the normalized D1stN (D1stN/D1stNm) as well as the normalized Féret diameter (D/Dm) versus the normalized shear stress (σ/σ_c) at two different experimental times: t = 1200 s and t = 3600 s. The first neighbor distance was normalized by the initial value (D1stNm) of sample σ = 0.1 Pa and the mean diameter is normalized by the initial value (Dm) of sample σ = 0.1 Pa. The critical shear stress was chosen at the end of the first Newtonian plateau, σ_c = 3 Pa as shown in Figure 4. The distance to the first neighbor decreased with the stress for the low and medium shear flows. For both regimes M1 and M2, as previously mentioned, aggregation predominated, unlike the high shear regime (M3) for which the first neighbor distance started to increase again. Figure 12 shows the corresponding

Cartesian representations for each case presented in Figure 11a. It can be seen that the particle aggregation increases with the shear stress up to 10 Pa; above 10 Pa, a further increase in the stress produced SU dispersion as shown in Figure 11a, even though images at 10, 100 and 200 Pa seem similar in Figure 12.

At this point, it is important to recall the definition of the structural units previously proposed. If we consider the SUs as small clusters composed of a few RuO_2 needles and Pd-Te spheres, the aggregates are clusters composed of SUs. Hence, the aggregates exhibit larger radii than the SUs. With image analysis, it was possible to extract the size of the SUs present in the sample, or more precisely their maximum Féret diameter. In Figure 11b, the surface percentage occupied by the SUs as a function of their diameters is plotted for all the 3600 s samples. At first, all samples show a similar size distribution. This confirms the SU hypothesis since all samples would have a majority of the surface occupied by small SUs of approximately 50 µm diameter dispersed in the matrix, corresponding to the average SU size previously measured by SEM in the glass [14]. It is paradoxically found that the average distance to the first neighbor at low and high shear scenarios are similar. However, it can be clarified by analyzing Figure 11b. For the medium and low shear stresses, contrary to the high shear stress regime, SUs present diameters greater than 300 and 450 µm, that is to say aggregates, can be observed. The same trend appears when the normalized mean diameter of the SUs (D/Dm) is plotted in Figure 11a as a function of the normalized shear stress for the 1200 and 3600 s experiments. After reaching a maximum size at 5 Pa the diameters drop, reaching a smaller SU size than at 0.1 Pa. Therefore, when comparing the D1stN for the low and high shear stress regimes, the values correspond to the D1stN between aggregates and structural units, respectively. Even though the values are similar, for higher shear stresses, the structure is a collection of small SUs.

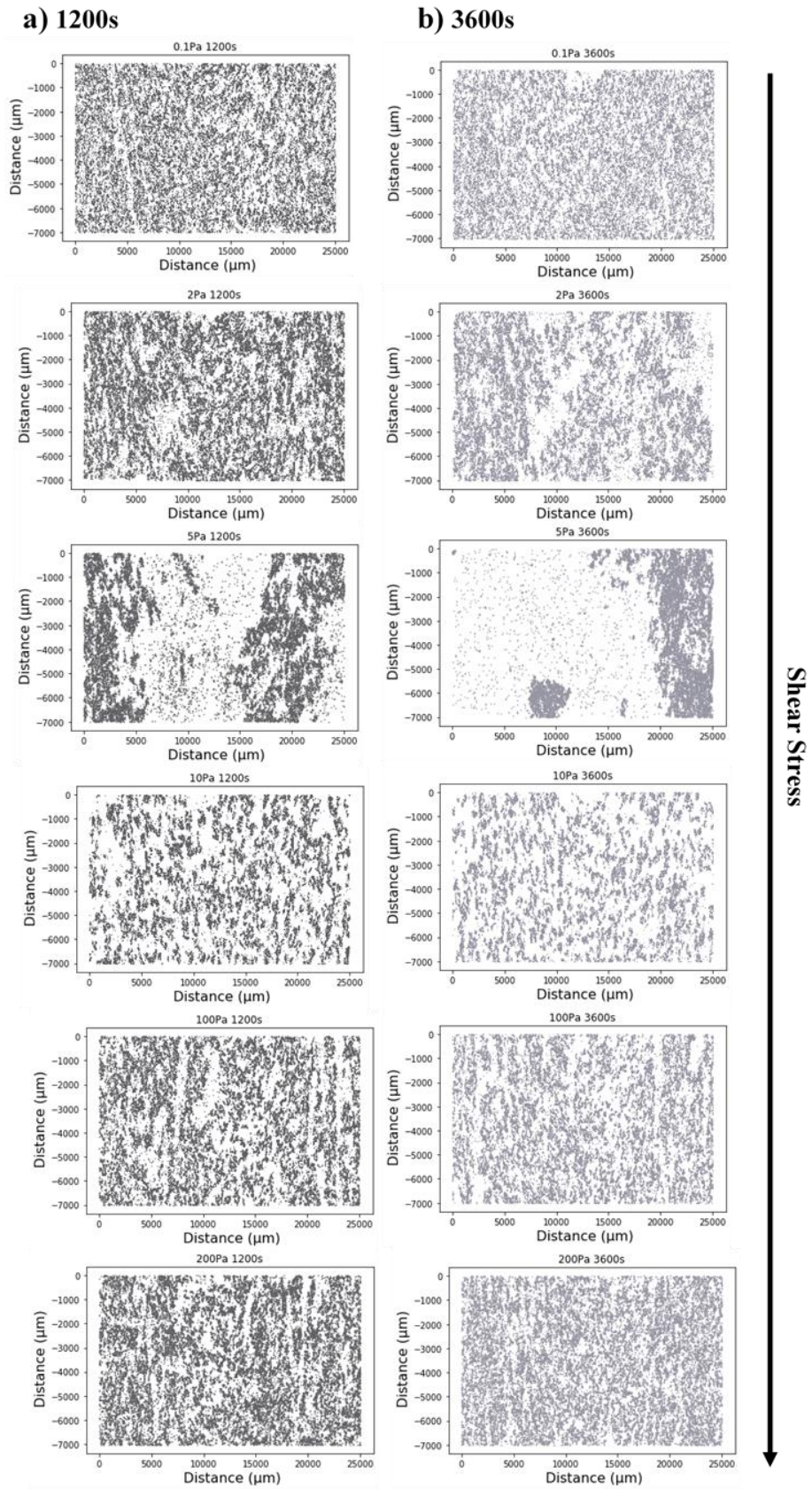

Figure 12 - Cartesian representations of the PGM structural units positioning in the top of the glass samples for all stresses at a) 1200 s and b) 3600 s.

3.5 Force balance and aggregation mechanisms

As mentioned earlier, the aggregation mechanisms studied in this work can be explained based on the DLVO theory [26], [27]. Although the three different mechanisms involve a balance between the forces acting on the material, for this work only two were considered: the hydrodynamic forces generated by the shear flow and the attractive van der Waals potential between the particles. It goes against the background of DLVO since double layer forces were ignored due to the difficulty in their evaluation [35][36]. Hydrodynamic and van der Waals forces were estimated through the relations provided by Allain *et al.* [35]. The hydrodynamic force was calculated as $F_H = \eta_f \dot{\gamma} R^2$, where η_f is the viscosity of the continuous phase, $\dot{\gamma}$ is the shear rate and R is the aggregate radius. For the van der Waals potential, the relation $F_{vdW} = \frac{\Lambda a}{12h^2}$, was considered, where Λ is the Hamaker constant, a is the particle radius and h is the mean distance between the particles.

Figure 13 shows the ratio between both forces as a function of $\dot{\gamma}/\dot{\gamma}_c$, where $\dot{\gamma}_c = \sigma_c/\eta_0$ is the critical shear rate at which the viscosity abruptly decreases (the critical stress σ_c and the low shear viscosity η_0 are indicated in Figure 4). The forces were approximated using the data obtained for the 3600 s experiments at all the shear stresses studied. To adapt the equations to experimental reality, the viscosity of the continuous matrix was considered as the viscosity of the simulated nuclear molten glass without PGM particles (η_f = 3.6 Pa.s) and the radius of the particles a as the mean size of the SUs ($a = 25$ μm). The aggregate radius (R) and the mean distance between the particles (h) are the mean Féret radius of the SUs and the D1stN for the 3600 s experiments, respectively (shown in Figure 11a). Since there is a lack of information on the Hamaker constant for silicate melts in the literature, a range of values was scanned.

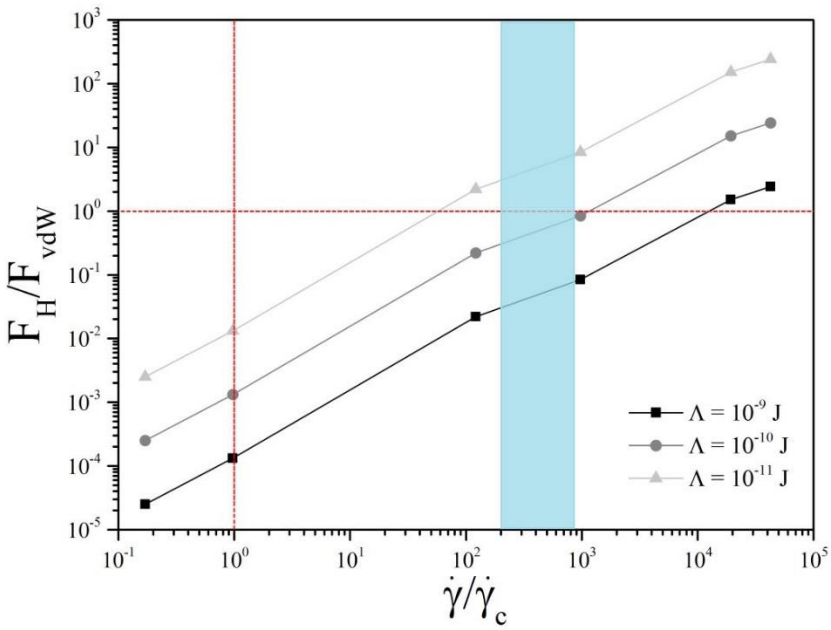

Figure 13 – The ratio between the hydrodynamic forces (F_H) and the van der Waals potential (F_{vdW}) as a function of $\dot{\gamma}/\dot{\gamma}_c$, for three different Hamaker constants. $\dot{\gamma}_c$ is the critical shear rate when the viscosity abruptly decreases.

When analyzing the graph, it can be seen that below the critical shear rate ($\dot{\gamma}/\dot{\gamma}_c \leq 1$), the van der Waals potential has a greater impact on the melt, as predicted for mechanism M1. For a shear above the critical value, the impact of the hydrodynamic force increases but the ratio F_H/F_{vdW} is still lower than one, indicating that hydrodynamic forces are not strong enough to break apart the aggregates completely and van der Waals attraction still dominates for particle reorganization in the melt. Hence the critical shear rate indicates only the limit between the two recognized rheological behaviors of the material (Newtonian and shear thinning). Note that the shear thinning behavior can be first induced by the orientation and organization of the aggregates and is not necessarily directly connected to the moment when the hydrodynamic forces surpass the binding forces between particles. Considering a Hamaker constant value between 10^{-10} and 10^{-11} J, the force balance corresponds to the hypothesis that the increase in the hydrodynamic forces and the beginning of the mechanism M3 occur when the shear is more than a hundred times the critical shear, corresponding to the shaded region of the graph. In terms of shear stress, it corresponds to more than 10 Pa, giving the smaller aggregates shown in Figure

12 that were formed after 3600 s due to the competition between the aggregation and dispersion of the SUs in the melt. It is important to stress that these Hamaker constant values are overestimated because the repulsive EDL force was neglected in the calculation. The introduction of this repulsive forces deserves a deeper investigation in the future.

4 Conclusions

The aggregation mechanisms of a simulated nuclear glass melt containing 3 wt.% of PGM particles were studied in this paper. The impact of the shear stress and time on the PGM particle aggregation degree was determined using a stress-imposed rheometer, working at high temperature, and an SEM image analysis method. Given the difficulties of in situ analysis at 1200 °C, a post-mortem approach was used after each sample was submitted at 1200 °C to different shear stresses and for different durations. These duration times were used to follow the evolution of the particles rearrangement with the viscosity, from the early stages of the regime to the steady state. For the same stress applied for different durations, the samples showed the same rheological behavior as a function of time, validating the reproducibility of the protocol implemented.

The image mosaics obtained for each sample were submitted to image analysis protocol in order to highlight the structural units (SUs) made of RuO_2 needles and Pd-Te spherical particles, and their distribution within the glass. This image analysis was an important tool to evidence the aggregation degree of each sample, highly influenced by the experiment time. Although visually the aggregation was clear, a numerical approach was developed in order to turn the distance between the first near neighbor of the SUs into a parameter to quantify the aggregation in each sample. The overall data showed that the PGM glass behaved in three different ways

depending on the flow regime imposed *i.e.*, low, medium and high shear flow regime. An explanation of the three mechanisms has been proposed in this work.

The three mechanisms are differentiated by the intensity of the forces acting on the particles. For the first regime, a combination of the low hydrodynamics forces and van der Waals attractive forces on the PGM particles contributes to the aggregation phenomenon, translated by the decrease in the distance between SUs. It affects the viscosity by increasing the effective volume fraction, leading to a higher viscosity at low shear rates. At a medium flow, the same forces are acting on the particles, but in a different ratio than the low shear regime: the hydrodynamic forces also have an impact by enhancing local reorganizations but are not strong enough to dissipate the SUs in the glass. The viscosity decreases significantly, but aggregation still occurs, which is shows by the continuous drop in distance values. At high shear flow, the SUs are completely dispersed in the melt due to the effects of the hydrodynamic forces, leading to a greaterr distance between the SUs and a lower viscosity. The experimental challenges of observing the aggregation kinetics of PGM particles in a glass melt were overcome thanks to a numerical approach that allows quantification of the evolution of aggregation and its impact to construct the general idea of what influences the phenomena. A balance between the hydrodynamic forces and the van der Waals potential was estimated using the data obtained to support our study's hypothesis. The information collected can be linked directly to the rheological behavior of the PGM glass, contributing to a deeper understanding of the material and consequently of the vitrification process.

5 Acknowledgements

The *Commissariat à l'Énergie Atomique et aux Énergies Alternatives* (CEA) and Orano are gratefully acknowledged for the financial support provided. The authors also would like to thank Sylvain Mure, Charlène Vallat and Henri-Pierre Brau for the valuable help in the

experimental part of the work, and for the fruitful discussions on SEM and image processing. Dr. Frank Trixler is also acknowledged for his important input in the DLVO discussion. Luiz Pereira acknowledges the support of the 2018 ADV 834225 (EAVESDROP) grant from the European Research Council.

6 References

[1] E. Vernaz, S. Gin, and C. Veyer, "Waste glass," *Compr. Nucl. Mater.*, vol. 5, no. January, pp. 451–483, 2012, doi: 10.1016/B978-0-08-056033-5.00107-5.

[2] R. F. Taylor, "Chemical engineering problems of radioactive waste fixation by vitrification," *Chem. Eng. Sci.*, vol. 40, no. 4, pp. 541–569, 1985, doi: 10.1016/0009-2509(85)80001-4.

[3] T. Akai, J. Nishii, M. Yamashita, and H. Yamanaka, "Chemical behavior of platinum-group metals in oxide glasses," *J. Non. Cryst. Solids*, vol. 222, pp. 304–309, 1997.

[4] C. Hanotin, J. Puig, M. Neyret, and P. Marchal, "Platinum group metal particles aggregation in nuclear glass melts under the effect of temperature," *J. Nucl. Mater.*, vol. 477, pp. 102–109, 2016, doi: 10.1016/j.jnucmat.2016.04.033.

[5] J. Puig, C. Hanotin, M. Neyret, and P. Marchal, "High temperature rheological study of borosilicate glasses containing platinum group metal particles by means of a mixer-type rheometer," *J. Nucl. Mater.*, vol. 469, pp. 112–119, 2016, doi: 10.1016/j.jnucmat.2015.11.053.

[6] C. Simonnet, A. Grandjean, and J. Phalippou, "Electrical behavior of platinum-group metals in glass-forming oxide melts," *J. Nucl. Mater.*, vol. 336, no. 2–3, pp. 243–250, 2005, doi: 10.1016/j.jnucmat.2004.09.019.

[7] R. B. Nuernberg, N. M. P. Machado, M. Malki, and M. Neyret, "Electrical behavior of RuO2-glass composites: The effect of RuO2 particle size on the percolation threshold,"

J. Nucl. Mater., vol. 546, p. 152777, 2021, doi: 10.1016/j.jnucmat.2020.152777.

[8] W. Grünewald, G. Roth, W. Tobie, K. Weiß, and S. Weisenburger, "The role of the platinum group elements ruthenium, rhodium and palladium in the vitrification of radioactive high level liquid waste using joule heated ceramic lined waste glass melters," *Glas. Technol. Eur. J. Glas. Sci. Technol. Part A*, vol. 49, no. 6, pp. 266–278, 2008.

[9] F. Pacaud, C. Fillet, and N. Jacquet-Francillon, "Effect of platinoids on French LWR reference glass properties," *Mater. Res. Soc. Symp. Proc.*, vol. 257, no. 3, pp. 161–167, 1992.

[10] R. B. Nuernberg, N. M. P. Machado, D. Jouglard, L. del Campo, M. Malki, and M. Neyret, "The origin of hysteresis in the electrical behavior of RuO2-glass composite melts," *J. Non. Cryst. Solids*, vol. 557, no. February, 2021, doi: 10.1016/j.jnoncrysol.2020.120596.

[11] L. Pereira *et al.*, "A Feedback Mechanism Between Crystals and Bubbles in a RuO2-Bearing Melt," *J. Non. Cryst. Solids*, 2022, doi: 10.1016/j.jnoncrysol.2022.121456.

[12] K. Uruga, T. Usami, T. Tsukada, S. Komamine, and E. Ochi, "Viscoplasticity of simulated high-level radioactive waste glass containing platinum group metal particles," *J. Nucl. Mater.*, vol. 452, no. 1–3, pp. 419–424, 2014, doi: 10.1016/j.jnucmat.2014.05.062.

[13] J. Puig, B. Penelon, P. Marchal, and M. Neyret, "Rheological Properties of Nuclear Glass Melt Containing Platinum Group Metals," *Procedia Mater. Sci.*, vol. 7, pp. 156–162, 2014, doi: 10.1016/j.mspro.2014.10.021.

[14] B. Luckscheiter, "Properties and behavior of the platinum group metals in the glass resulting from the vitrification of simulated nuclear fuel reprocessing waste," *J. Mater. Res.*, vol. 6, no. 12, pp. 2535–2546, 1991, doi: 10.1557/JMR.1991.2535.

[15] Y. Yue and R. Brückner, "A new description and interpretation of the flow behaviour of

glass forming melts," *J. Non. Cryst. Solids*, vol. 180, no. 1, pp. 66–79, 1994, doi: 10.1016/0022-3093(94)90398-0.

[16] F. Babick, *Suspensions of Colloidal Particles and Aggregates*, vol. 20. Dresden, Germany: Springer International Publishing, 2016.

[17] C. Bower, C. Washington, and T. S. Purewal, "The use of image analysis to characterize aggregates in a shear field," *Colloids Surfaces A Physicochem. Eng. Asp.*, vol. 127, no. 1–3, pp. 105–112, 1997, doi: 10.1016/S0927-7757(96)03945-3.

[18] A. Kurokawa, V. Vidal, K. Kurita, T. Divoux, and S. Manneville, "Avalanche-like fluidization of a non-Brownian particle gel," *Soft Matter*, vol. 11, no. 46, pp. 9026–9037, 2015, doi: 10.1039/c5sm01259g.

[19] S. Deboeuf, N. Lenoir, D. Hautemayou, M. Bornert, F. Blanc, and G. Ovarlez, "Imaging non-Brownian particle suspensions with X-ray tomography: Application to the microstructure of Newtonian and viscoplastic suspensions," *J. Rheol. (N. Y. N. Y).*, vol. 62, no. 2, pp. 643–663, 2018, doi: 10.1122/1.4994081.

[20] T. Advocat, J. L. Dussossoy, and V. Petitjean, "Vitrification des déchets radioactifs et appareillage," *Les Tech. l'Ingénieur*, vol. 33, pp. 0–27, 2008.

[21] M. Bousmina, A.-S. Chrissemant, L. Choplin, A. Aït-Kadi, and P. Marchal, "Quantitative Analysis of Mixer-Type Rheometers using the Couette Analogy," *Can. J. Chem. Eng.*, vol. 80, no. December, pp. 1166–1174, 2010, doi: 10.1002/cjce.5450800618.

[22] Bousmina M.; A. Aït-Kadi and J.B. Faisant, "Determination of Shear Rate and Viscosity from Batch Mixer Data: Theoretical and Experimental Results," *J. Rheol*, vol. 43, p. 1999, 1999.

[23] W. L. Wang, J. Q. Bi, K. N. Sun, M. Du, N. N. Long, and Y. J. Bai, "Thermal shock resistance behavior of alumina ceramics incorporated with boron nitride nanotubes," *J.*

Am. Ceram. Soc., vol. 94, no. 8, pp. 2304–2307, 2011, doi: 10.1111/j.1551-2916.2011.04658.x.

[24] O. Delattre, E. Régnier, S. Schuller, M. Allix, and G. Matzen, "Image analysis study of crystallization in two glass compositions of nuclear interest," *J. Non. Cryst. Solids*, vol. 379, pp. 112–122, 2013, doi: 10.1016/j.jnoncrysol.2013.07.029.

[25] J. Fournier-Renaud, "Cinétiques de dissolution des cristaux dans les silicates fondus – contexte des verres nucléaires," Université Montpellier, 2017.

[26] B. Derjaguin and L. Landau, "Theory of the stability of strongly charged lyophobic sols and of the adhesion of strongly charged particles in solutions of electrolytes," *Prog. Surf. Sci.*, vol. 43, no. 1–4, pp. 30–59, 1993, doi: 10.1016/0079-6816(93)90013-L.

[27] C. E. Marshall, "'Theory of the stability of lyophobic colloids. The interaction of particles having an electric double layer.' E. J. W. Verwey and J. T. G. Overbeek, with the collaboration of K. van Ness. Elsevier, New York-Amsterdam, 1948, 216 pp.," *J. Polym. Sci.*, vol. 4, no. 3, pp. 413–414, Jun. 1949, doi: 10.1002/pol.1949.120040321.

[28] W. R. Richmond, R. L. Jones, and P. D. Fawell, "The relationship between particle aggregation and rheology in mixed silica-titania suspensions," *Chem. Eng. J.*, vol. 71, no. 1, pp. 67–75, 1998, doi: 10.1016/S1385-8947(98)00105-3.

[29] D. Quemada, "Rheological modelling of complex fluids: II. Shear thickening behavior due to shear induced flocculation," *EPJ Appl. Phys.*, vol. 2, no. 2, pp. 175–181, 1998, doi: 10.1051/epjap:1998170.

[30] H. A. Barnes, *A Handbook of Elementary Rheology*. The University of Wales- Institute of Non-Newtonian Fluid Mechanics, Department of Mathematics, 2000.

[31] D. B. Genovese, "Shear rheology of hard-sphere, dispersed, and aggregated suspensions, and filler-matrix composites," *Adv. Colloid Interface Sci.*, vol. 171–172, pp. 1–16, 2012, doi: 10.1016/j.cis.2011.12.005.

[32] P. Snabre and P. Mills, “Rheology of concentrated suspensions of viscoelastic particles,” *Colloids Surfaces A Physicochem. Eng. Asp.*, vol. 152, no. 1–2, pp. 79–88, 1999, doi: 10.1016/S0927-7757(98)00619-0.

[33] V. A. Tolpekin, M. H. G. Duits, D. Van Den Ende, and J. Mellema, “Aggregation and breakup of colloidal particle aggregates in shear flow, studied with video microscopy,” *Langmuir*, vol. 20, no. 7, pp. 2614–2627, 2004, doi: 10.1021/la035758l.

[34] S. Herminghaus, *Wet Granular Matter*, vol. 6. WORLD SCIENTIFIC, 2013.

[35] C. Allain, M. Cloitre, and F. Parisse, “Settling by cluster deposition in aggregating colloidal suspensions,” *J. Colloid Interface Sci.*, vol. 178, no. 2, pp. 411–416, 1996, doi: 10.1006/jcis.1996.0135.

[36] F. E. Torres, W. B. Russel, and W. R. Schowalter, “Floc structure and growth kinetics for rapid shear coagulation of polystyrene colloids,” *J. Colloid Interface Sci.*, vol. 142, no. 2, pp. 554–574, 1991, doi: 10.1016/0021-9797(91)90086-N.